Article

Signal Outages of CSMA/CA-Based Wireless Networks with Different AP Densities

Soohyun Cho (ID)

Department of General Studies, Hongik University, Seoul 04066, Korea; cho.soohyun@hongik.ac.kr;
Tel.: +82-2-320-3383

check for updates

Abstract: In wireless networks, users may experience outages owing to low received signal strength. Divergent from other research, we investigate the outages for users of CSMA/CA-based wireless networks when multiple access points (APs) and multiple users are randomly positioned in a given area. We model the locations of the APs and users using independent homogeneous Poisson point processes (PPPs), and analyze the signal outage probabilities of users when there are different numbers of access points, as well as when different modulation and coding schemes (MCSs) are used for communication. We also investigate heterogeneous CSMA/CA-based wireless networks, wherein the APs use different transmit powers. Then, we evaluate the results and compare the signal outage rates of users with the signal-to-interference-plus-noise ratio (SINR) outage rates of users in both homogeneous and heterogeneous IEEE 802.11a wireless networks using extensive event-driven simulations. The simulation results validate our analysis on the signal outages of users in multi-cell, multi-user wireless networking environments, and show that a significant portion of outages are caused by the signal outages when AP densities are low and high MCS levels are used for communication.

Keywords: signal outage; SINR outage; IEEE 802.11; CSMA/CA; Poisson point process

1. Introduction

Emerging Internet of Things (IoT-) based services [1], such as smart homes [2] and smart vehicles [3], require technical development in various fields such as power control [4] and privacy [5]. However, to accommodate the expected large number of IoT devices, we believe that carrier-sense multiple access with collision avoidance (CSMA/CA-) based wireless networks, such as IEEE 802.11 [6] and IEEE 802.15.4 [7] standards, would be a convenient choice to achieve the connectivity of IoT devices because of the high penetration of the CSMA/CA-based wireless networks in many places.

Besides the wide installation of IEEE 802.11 access points (APs) by end users or owners of businesses such as shopping malls, recently several metropolitan cities have begun to build massive IEEE 802.11 wireless networks not only for some popular locations, but for all public spaces, as a form of public service [8]. However, even in urban areas of developed countries, while the densities of IEEE 802.11 APs are high in most areas, there are regions called dead spots [9], where users experience poor performance owing to low radio signal strengths (we call these signal outages). Because the usual transmit power of IEEE 802.11 APs is much smaller than that of cellular base stations, users of IEEE 802.11 wireless networks may experience poor performances or outages due to power shortages of the received radio signals more often than when using cellular networks (The transmit power of macro base stations in cellular networks is usually 40 W, while the transmit power of IEEE 802.11 APs is usually 100 or 200 mW.).

Furthermore, in wireless networks, outages also occur when the signal-to-interference-plus-noise ratios (SINRs) of received packets are not sufficiently high to correctly demodulate the packets for the

modulation and coding scheme (MCS) used between senders and receivers (this is called the SINR outage). Thus, because of the (unorganized) dense installation of IEEE 802.11 APs and the popularity of using IEEE 802.11 wireless networks, users of IEEE 802.11 wireless networks may experience poor performance from the SINR outages in crowed areas, although the received radio signal strengths from their serving APs are high.

Recently, heterogeneous wireless networks (HetNets) [10] are considered as one of the key technologies for future wireless networks. The heterogeneous wireless networks refer to wireless networks that are composed of heterogeneous cells such as macro-cells and small cells (i.e., a combination of APs having different transmit powers) [11]. For cellular networks that use technologies such as LTE, macro-cells usually contribute to realizing a wide coverage area in which a minimum throughput is guaranteed, while small cells (also known as femto-cells or pico-cells) are used to build hot-spot zones that can offload the load of the busy macro-cells.

However, the use of heterogeneous CSMA/CA-based wireless networks has not attracted much attention compared to heterogeneous cellular networks. This is mainly because the different transmit powers of APs in CSMA/CA-based wireless networks may introduce unfairness among users, and most IEEE 802.11 wireless networks operate without central management. Nonetheless, because the coverage areas of small cells are smaller than those of macro-cells, services such as location-based services or IoT-based services may work better when many small cells are around the wireless devices. Furthermore, because virtually all smartphones can use IEEE 802.11 wireless networks, and an increasing number of consumer products in markets are equipped with IEEE 802.11 wireless networking capability, we investigate the signal outages and SINR outages of users in heterogeneous IEEE 802.11 wireless networks as well as the homogeneous cases.

1.1. Related Work

Many researchers have employed theories obtained from stochastic geometry [12], such as homogeneous Poisson point processes (PPPs) [13], to achieve mathematically tractable formulas for various kinds of wireless network-related issues, such as to determine SINR distributions and SINR outage (or coverage) probabilities [14] for a given target SINR, as well as the transmission capacity [15] for cellular networks or wireless networks with simple medium access schemes such as the slotted ALOHA.

In [16], the authors analyze the probabilities of inactive base stations using densities of both base stations and users, and they used the results to derive the service success probabilities in cellular networks. In [17], the authors analyze coverage probabilities and average ergodic rates in heterogeneous cellular networks using stochastic geometry. In [18], the authors analyze offloading between different radio technologies, such as cellular networks and IEEE 802.11 wireless networks. In [19], the authors propose the improved estimations of cell-size distributions in heterogeneous networks. In [20], the authors analyze the performances of closed-access heterogeneous cellular networks.

Other forms of distributions, such as the uniform distribution, and the mobility of nodes are also considered by many researchers. In [21], the authors analyze the distribution of the interference when nodes are uniformly distributed in a finite area using traffic patterns similar to those from the slotted ALOHA. In [22], the authors propose including the angular directions of antennas in the analysis of the peer-to-peer networks with uniformly distributed sources. In [23], the authors propose using adaptive antenna arrays to improve the multi-packet communications in IEEE 802.11 heterogeneous networks (In this study, the heterogeneous networks refer to the wireless networks of nodes with different antenna systems.). In [24], the authors analyze the SINR outage of users using the nearest (dominant) interferer when nodes are randomly distributed with both uniform and non-uniform densities. In [25], the authors analyze the spatial distribution of the nodes in the random waypoint mobility model for wireless ad-hoc networks. In [26], the authors analyze the interference and outages in mobile random networks of a simple medium access scheme.

Compared to the analysis of cellular networks or simple medium access schemes, the analysis of CSMA/CA-based wireless networks with stochastic geometry appears to be more challenging mainly because of the collision avoidance mechanism adopted in CSMA/CA. In [27], the authors propose a modified Matérn point process by thinning the original PPP distributions of nodes. They show the changes of SINR coverage probabilities with various PPP densities of APs. In [28], the authors show that with Matérn hard-core process type II, it is better to explain the interference in CSMA/CA-based wireless networks than with the type I. In [29], the authors show the distribution of the throughputs achieved by APs in CSMA/CA-based wireless networks with different AP densities and different carrier-sensing threshold values. In [30], the authors propose a modified Matérn hard-core process to mitigate underestimation problems obtained by Matérn hard-core process type II.

For the efficient routing in wireless/wired networks, a lot of research has been conducted for various fields such as ad-hoc routings for wireless sensor networks, and recently, finding paths for cloud-based services. In [31], the authors propose an energy efficient routing algorithm using dynamic programming to solve the routing problem in wireless sensor networks. In [32], the authors propose a multi-cloud framework to increase energy efficiency and other performance metrics such as QoS. In [33,34], the authors propose a framework to find energy efficient routing paths to the requested resources in cloud-based services.

1.2. Contribution and Methodology

Most of the studies on wireless networks mentioned in the related work focus on the analysis of the SINR outages or improving SINR coverages in cellular networks or wireless networks with simple medium access schemes. In addition, many of the studies use simple networking scenarios, such as a single receiver in the center or within the same distance for all the sender-receiver pairs to mitigate the difficulty in the analysis. Our work is different from these studies mainly because we consider the outages in multi-cell, multi-user environments for more realistic CSMA/CA-based wireless networking scenarios.

In the multi-cell, multi-user environments, more than one user can associate with the same AP, and the distances between the users and their serving APs are generally different. In these environments, interference can come not only from the contending users sharing the same serving AP but also from other APs and users in the other cells. Furthermore, we differentiate the signal outages from the SINR outages, and analyze the signal outages when different numbers of users and APs are randomly positioned with different PPP densities in a given area, and when different MCS levels are used for communication between them. In addition, we investigate the impact of the signal outages on the SINR outages of users in both homogeneous and heterogeneous networks using extensive event-driven simulations.

For the geographical distributions of the IEEE 802.11 APs and users (i.e., wireless user devices) in both homogeneous and heterogeneous networks, we adopt the homogeneous PPPs because IEEE 802.11 APs can be independently and easily installed (and operated) by end users. For the simulations, we use the event-driven network simulator ns-2 (version 2.35) [35] and IEEE802.11Ext module [36] in the ns-2 to simulate IEEE 802.11a [37] wireless networks. We adopt the IEEE802.11Ext module because it uses not only the signal strengths and the arrival times of packets but also the sizes and the MCS levels of the packets (i.e., packet duration) to accurately calculate the cumulative interference [38] and the SINRs of packets while they are being received. We use IEEE 802.11a in this paper because it is one of the two standards (the other standard is IEEE 802.11p for a vehicular communication; we do not use the standard because mobility is out of the scope of this paper) whose PHY/MAC configuration parameters are provided by the authors of the IEEE802.11Ext module [39], and we believe that we can capture the behavior of CSMA/CA-based wireless networks by using it, although it is not the state-of-the-art technology.

The remainder of this paper is organized as follows: In Section 2, we define the signal outages and the maximum allowed distances between users and their associated APs in order to satisfy the

minimum SINR requirements of the MCS levels. In Section 3, we analyze signal outage probabilities of users in homogeneous wireless networks and evaluate the analysis using simulation results. In addition, we compare the signal outages with SINR outages of users in CSMA/CA-based wireless networks by performing extensive simulations. In Section 4, we analyze the signal outage probabilities of users in heterogeneous wireless networks and compare the results with the SINR outages of users in heterogeneous CSMA/CA-based wireless networks. In Section 5, we show simulation results when transmitted packets experience the Rayleigh fading, and the RTS/CTS scheme is enabled in simulations. Section 6 concludes this paper.

2. Maximum Allowed Distances and Signal Outages

2.1. Radio Transmission Model

We consider a two-dimensional (2D) Euclidean plane, and we model the spatial distributions of APs and users with independent homogeneous Poisson point processes for multi-cell, multi-user wireless networking environments. In this paper, we consider only single-channel, half-duplexed wireless networks. To calculate the signal strength (i.e., power) and SINR of a received packet, we use a simple radio transmission model similar to the one used in [40]: the signal strength P_i of packets received by a user i located at x_i sent from an AP k located at x_k is modeled as

$$P_i = A \cdot h \cdot P_t \|x_i - x_k\|^{-\alpha}, \tag{1}$$

where A is a constant that represents communication environments such as antenna heights. h is to model the short-term fading effects, which is assumed as the Rayleigh fading with unit mean (However, in simulations, the fading is applied only when its use is explicitly stated. Otherwise, $h = 1$.) (i.e., $h \sim exp(1)$ as $E[h] = 1$) similarly to [18]. $\| \cdot \|$ represents the Euclidean norm (If the distance between a sender and a receiver is less than 1 m, we set the Euclidean norm to 1 as nodes can be arbitrarily close to each other because of the property of homogeneous PPPs.). α is the path-loss exponent, which is fixed at 4 in this paper. P_t represents the transmit power of nodes (i.e., APs and users). In homogeneous networks, we assume that all APs use the same transmit power P_t. In heterogeneous networks, we use P_{tn} to represent the transmit power of tier-n APs, and all APs of the tier-n use the same transmit power of P_{tn}.

For the simulation of the radio transmission model, we use the `TwoRayGround` module [41] in the ns-2, which is modified (Use of the free space model [41] is disabled.) to use the fixed path-loss exponent (i.e., $\alpha = 4$.). In the `TwoRayGround` module, the constant A is set to the product of the squared antenna heights of the sender and the receiver in the absence of the antenna gain. Thus, in this paper, A is ∼5.06 because we assume that the heights of the antennas of both senders and receivers are 1.5 m and there is no antenna gain. All antennas are assumed to be omnidirectional. The carrier frequency of the simulated IEEE 802.11a is set to 5.18 GHz, and it is reflected in the propagation times of the packets between nodes by the IEEE802.11Ext module in the ns-2.

Before starting communications, we assume that all users are connected to (or associated with) the APs of the strongest received signal strength using Equation (1) even if the signal strengths are too low for actual communication. For the directions of traffic, we consider only downlink data flows from APs to users (i.e., there are no direct data flows between users.). Therefore, if we assume that user i is associated with an AP k located in x_k, all signals sensed by user i, except for those from the AP k, are interpreted as interference. We model the interference I_i experienced by user i located at x_i as

$$I_i = \sum_{j \neq k} A \cdot h \cdot P_t \|x_i - x_j\|^{-\alpha} \mathbb{1}_{\{j \text{ interferes with } k\}}, \tag{2}$$

where x_j indicates the locations of APs or other users whose signals are sensed by user i. $\mathbb{1}$ is the indicator function, and it represents the presence of the interfering packets while the desired packets from AP k are being received. Note that the IEEE802.11Ext module calculates the cumulative power [38]

using the arrival times and the durations of the interfering packets to measure the aggregated interference from multiple, concurrent interfering packets. Furthermore, because the receivers of CSMA/CA-based wireless networks transmit acknowledgment (ACK) frames when they correctly receive data packets, not only the data packets from other APs but also the ACK frames from other users contribute to the interference because we assume single-channel, half-duplexed CSMA/CA-based wireless networks.

Using Equations (1) and (2), we model the SINR τ_i of a packet received by user *i* from its associated AP *k* as

$$\tau_i = \frac{P_i}{I_i + W},\tag{3}$$

where *W* is the thermal noise power at the receivers, and it is assumed to be -126 dBW which is suggested by the authors of the IEEE802.11Ext module [39].

2.2. MCS and Maximum Allowed Distances

CSMA/CA-based wireless networks, such as IEEE 802.11 standards, use various MCSs to effectively utilize wireless networks; nodes can send packets at high speed using high MCS levels. However, the packets sent with the high MCS levels require high SINRs for the correct demodulation of the packets by the receivers. As an example, the IEEE 802.11a standard uses eight MCS levels, each of which is required to satisfy its own minimum SINR condition [37]. However, the `IEEE 802_11Ext` module that we used in this study to simulate IEEE 802.11a wireless networks supports only four MCS levels [39], as shown in Table 1. In the table, we also show the (physical layer) transmission speeds and the minimum SINR requirements of the four MCS levels.

Table 1. MCS levels, transmission speed, and minimum SINR requirements of IEEE802.11Ext module.

MCS Level *k*	MCS	Transmission Speed	Min. SINR τ_k (dB)
0	BPSK, 1/2 coding	6 Mbps	5
1	QPSK, 1/2 coding	12 Mbps	8
2	16QAM, 1/2 coding	24 Mbps	15
3	64QAM, 3/4 coding	54 Mbps	25

From the minimum SINR requirement τ_k of each MCS level *k* and the assumed noise power (i.e., *W* = -126 dBW), we can find the minimum received signal strength requirement P_k of each MCS level by setting I_i to zero in Equation (3) as below:

$$P_k = \tau_k \cdot W.\tag{4}$$

Hence, the minimum received signal strength requirement for each MCS level in Table 1 is about -121 dBW, -118 dBW, -111 dBW, and -101 dBW for MCS 0, MCS 1, MCS 2, and MCS 3, respectively (note that the minimum received signal strength requirements can be obtained by simply adding the given noise power to the minimum SINR requirement of each MCS level in the dB scale). These minimum received signal strength requirements for the four MCS levels are shown in Table 2.

Using the minimum received signal strength requirement of each MCS level and the radio transmission model in Equation (1), we define the maximum distance D_k allowed between a user and its serving AP for each MCS level k as below:

$$
\begin{aligned}
D_k &= \left(\frac{P_k}{A \cdot E[h] \cdot P_t} \right)^{-1/\alpha} \\
&= \left(\frac{A \cdot E[h] \cdot P_t}{\tau_k \cdot W} \right)^{1/\alpha} \\
&= \left(\frac{A \cdot P_t}{\tau_k \cdot W} \right)^{1/\alpha},
\end{aligned} \tag{5}
$$

because $E[h] = 1$ by the assumption. Hence, as an example, if we set P_t to 100 mW, the maximum allowed distance of each MCS level is about 894 m, 752 m, 502 m, and 284 m for MCS 0, MCS 1, MCS 2, and MCS 3, respectively. These results are shown next to the minimum received signal strength requirement of each MCS level in Table 2.

Table 2. Minimum signal strength requirement P_k and maximum allowed distance D_k when P_t = 100 mW and $W = -126$ dBW.

MCS Level k	Min. Signal Strength P_k (dBW)	Max. Distance D_k (m)
0	−121	893.5
1	−118	751.8
2	−111	502.4
3	−101	283.5

To demonstrate the impact of the maximum allowed distances, we run ns-2 simulations with one user and one AP using different MCS levels. In the simulation, the AP sends constant bit rate (CBR) traffic of 30 Mbps to the user while the user is moving away from the AP in an area of 2000 m × 2000 m for a simulation time of 10 s. Both the AP and the user use a transmit power of 100 mW.

In Figure 1, we show the changes in the throughputs achieved by the user when different MCS levels are used between the AP and the user. The simulation results in the figure clearly show that the user needs to be inside the maximum allowed distance of each MCS level from the AP to achieve the corresponding throughput of the MCS level (The achieved throughputs shown in Figure 1 are less than the transmission speeds of the MCS levels shown in Table 1 because we measured the application throughputs, and the overhead of the CSMA/CA mechanism consumes bandwidth.). Otherwise, the user achieves no throughput (i.e., outages occur). This is because the packets that arrived beyond the maximum allowed distance of each MCS level have lower SINR values than the required minimum SINR although there is no interference.

We refer to the outage caused by the violation of the minimum received signal strength requirement as the *signal outage*, and we differentiate it from the SINR outage because it is caused by a shortage of the received signal power, and not by the interference.
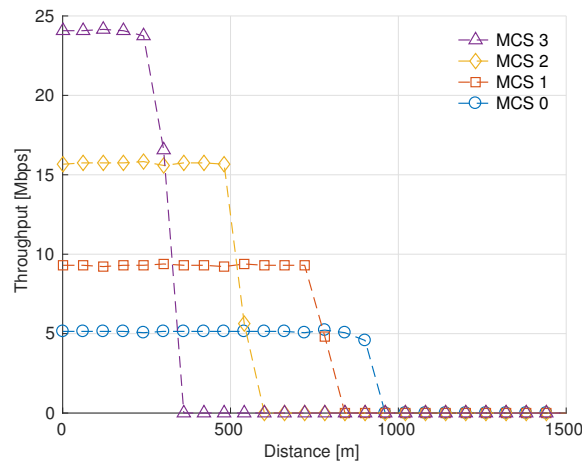
Figure 1. Changes of achieved throughputs versus distances from AP with different MCS levels.

3. Homogeneous Networks

To investigate the signal outages and the SINR outages in homogeneous IEEE 802.11 wireless networks, we assume that all APs and users use the same transmit power P_t of 100 mW.

3.1. Distances between Access Points and Users

Because we model the geographical distributions of both APs and users with independent homogeneous PPPs, the distributions of the distances between users and their closest APs with PPP density λ are well-known [12]: the complementary cumulative distribution function (CCDF), $P(R > r)$, and probability density function (PDF), $f_R(r)$, of a random variable R for the distances are respectively given as

$$P(R > r) = e^{-\lambda \pi r^2}, \tag{6}$$

$$f_R(r) = 2\lambda \pi r e^{-\lambda \pi r^2}. \tag{7}$$

From the PDF in Equation (7), the expected distance of a user to its closest AP, $E[R]$, can be expressed as

$$\begin{aligned}
E[R] &= \int_0^\infty r \cdot 2\lambda \pi r e^{-\lambda \pi r^2} dr \\
&= \lambda \pi \int_0^\infty v^{1/2} e^{-\lambda \pi v} dv \\
&= \lambda \pi \frac{1}{2\pi \lambda^{\frac{3}{2}}} \\
&= \frac{1}{2\sqrt{\lambda}}.
\end{aligned} \tag{8}$$

As a demonstration, in Figure 2a, we show the simulation results of the average distances between the users and their closest APs for APs with different PPP densities. For the simulations, we increased both the number of APs and the number of users from two to 60 (i.e., 2, 4, 6, 10, 20, 30, 40, and 60) in a circular area with a radius of 1000 m. The simulation results are averaged values from 100-time repetitions with different seeds for randomness. In Figure 2b, we also show the Voronoi diagram [42] from one realization of PPPs with 30 APs and 30 users. The red arrows in the figure show the connectivity and directions of the flows between users and their serving APs.
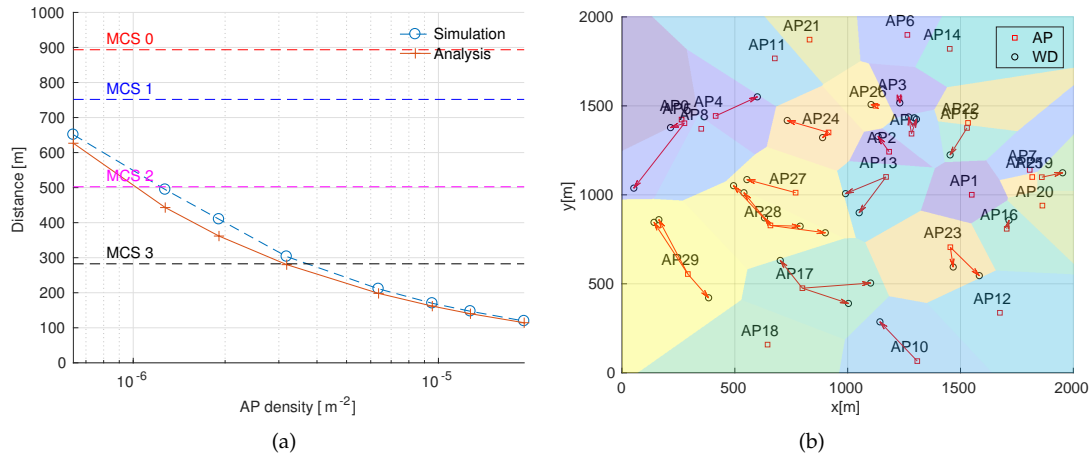
Figure 2. (**a**) Average distances between users and their closest APs for different densities. (**b**) Voronoi diagram of 30 APs and 30 wireless user devices (WDs).

Figure 2a shows that the simulation results follow the analysis of Equation (8). In Figure 2a, we also show the maximum allowed distances of the four MCS levels in Table 2 with dashed lines. From the figure, we can see that the maximum allowed distances for MCS 2 and MCS 3 are not satisfied (on average) when the densities are low. The simulation results in Figure 2a clearly show that when high MCS levels, such as MCS 2 or MCS 3, are used in such sparse environments, signal outages can occur by the low received signal strengths regardless of the existence of the inference.

However, as may be seen from Figure 2b, the users close to the edge of the circular area tend to be far from their serving APs. This is because the APs and users are randomly positioned using PPPs only in the circular area with a radius of 1000 m. This effect is called the edge effect [27], which occurs when PPPs are simulated in a bounded area like ours. We can see that the edge effect is reflected in Figure 2a, in which the simulation results show slightly higher distances than the analysis in low AP density settings.

3.2. Signal Outages

With the given homogeneous PPP density λ and the minimum SINR requirement τ_k of MCS level k, we derive an estimate for the probability of the signal outages in MCS level k, PO_k, using Equations (5) and (6) as follows:

$$
\begin{aligned}
PO_k &= P(R > D_k) \\
&= e^{-\lambda \pi D_k^2} \\
&= e^{-\lambda \pi \left(\frac{AP_t}{\tau_k \cdot W} \right)^{\frac{2}{\alpha}}}.
\end{aligned}
\tag{9}
$$

This signal outage probability can be considered as the lowest bound of the SINR outage probability because the interference-plus-noise power cannot be less than the noise power itself.

Owing to the property of the homogeneous PPP, when the density of the APs, λ_a, and the density of the users, λ_u, are different, the estimate of the signal outage probability for an MCS level k can be expressed using only λ_a if they are independent from each other, as follows:

$$
PO_k = e^{-\lambda_a \pi \left(\frac{AP_t}{\tau_k \cdot W} \right)^{\frac{2}{\alpha}}}.
\tag{10}
$$

Thus, the estimate of the signal outage probability is not affected by the density of users if they are distributed with another independent homogeneous PPP. Note that this independence from the user density also holds for the heterogeneous networks in Section 4.

To evaluate the analysis of signal outages in Equation (9), we show simulation results for different PPP densities and MCS levels in Figure 3a. In the simulations, for each MCS level, both the number of APs and users are increased from two to 60 as before. The simulation results are averaged values from 100-time repetitions. From the simulation results and the analytic data from Equation (9) shown together in the figure, we can see that the simulation results follow the estimated signal outage probabilities.
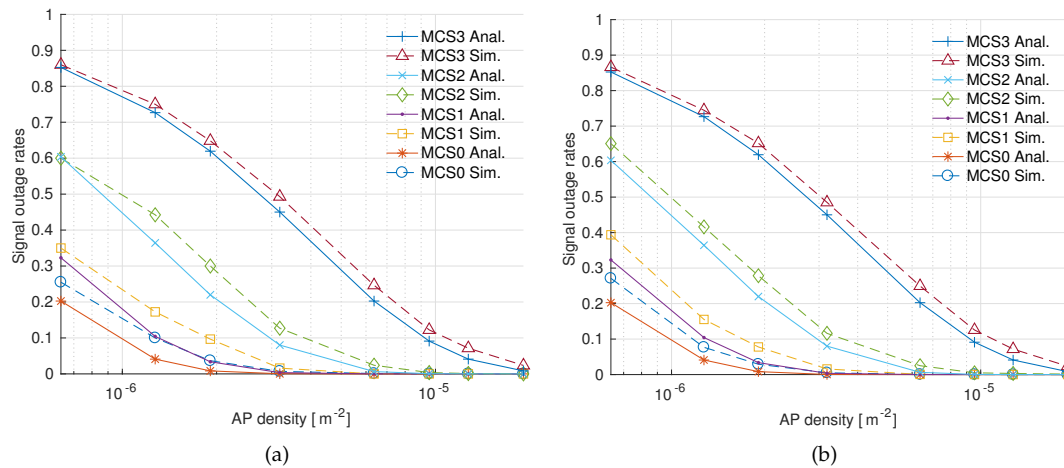
Figure 3. (**a**) Signal outage rates of users with different MCS levels and different numbers of APs. (**b**) Signal outage rates of users when the number of users is fixed at 60.

In addition, to validate the independence of the signal outage probability from the user densities, we show the simulation results of the signal outages in Figure 3b when the number of users is fixed, but with different MCS levels and different AP densities: The number of users remains fixed at 60 while the number of APs increases from two to 60. From the simulation results and the analytic data from Equation (10) shown together in the figure, we can see that the simulation results follow the analysis of the signal outage probabilities, which is similar to the results in Figure 3a.

However, the simulation results in both Figure 3a,b show a pattern of slightly higher signal outages from the analysis. The pattern in the figures can also be observed in other simulation results in this paper and we believe that they are caused by the edge effect mentioned in Section 3.1.

3.3. Comparison with SINR Outages

In this section, we investigate the impact of signal outages on the SINR outages for APs with different PPP densities and different MCS levels using extensive ns-2 simulations. In the ns-2 simulations, all participants (i.e., APs and user devices) use the same MCS level for communication during the 5-s-long simulation time in a circular area with a radius of 1000 m. All of the users are assumed to be connected to their closest (in homogeneous networks, the node with the strongest received power is the same as the closest node) APs before starting communications. APs are continuously backlogged (i.e., saturated) by CBR traffic of 30 Mbps to each user associated with them. The packet size of the CBR traffic is set to 1000 bytes.

All participating nodes use the distributed coordination function (DCF) [6] to avoid collisions. To set up bi-directional, one-hop path between APs and their associated users, we use No Ad-hoc Routing Agent (NOAH) [43] to explicitly remove the possibility of ad-hoc routing among nodes. The request to send/clear to send (RTS/CTS) scheme is not used except when its use is explicitly stated. The queue sizes of output ports in APs and user devices were set to 50 packets. For the simulations,

other parameters were set to the proposed values (`PowerMonitorThresh_` was set to -129 dBW and `CSThresh_` was set to -112 dBW) in [39] for IEEE 802.11a wireless networks unless stated otherwise.

During each ns-2 simulation run, we record all of the signal strengths and SINRs of all the packets when they arrive at their target nodes, and we calculate their average values during the simulation time for every user in the simulation. Some of the data packets cannot be received successfully by the users, either because of the low received signal strength (i.e., signal outage events occur) or because of the low SINR (i.e., SINR outage events occur) of the packets when they arrive at their target nodes. However, note that the SINR outage events include the signal outage events because the minimum requirement for an MCS level cannot be satisfied if the received signal strength of the packet does not satisfy the minimum signal strength requirement of the MCS level.

If the averaged received signal strengths of all the packets that arrived at a user during the simulation time is smaller than the minimum strength for the used MCS level, the user is marked as a user affected by signal outages (i.e., signal-outage user). If the averaged SINRs of all of the packets that arrived at a user are smaller than the minimum SINR requirement for the used MCS level, the user is marked as a user affected by SINR outages (i.e., SINR-outage user).

After each simulation run, we calculate the rates of signal-outage users by counting the number of signal-outage users from among the total number of users in the simulation. Similarly, we calculate the rates of the SINR-outage users by counting the number of SINR-outage users from among the total number of users in the simulation. For each scenario involving a different AP density and MCS level, we calculate averaged values from the rates of the signal-outage users and the SINR-outage users from 100 simulation runs.

In Figure 4a, we show the simulation results of the signal outage rates and the SINR outage rates with different AP densities and different MCS levels when $\lambda_u = \lambda_a$. From the figure, we can see that the signal outages are dominant in the SINR outages in the scenarios with low AP densities, but they are less dominant with higher AP densities. Note that the SINR outages in Figure 4a show similar patterns reported in [27] if they are converted to SINR coverages. However, they are different from those of the cellular networks [17] owing to the exponential back-off algorithm of the CSMA/CA mechanism used in IEEE 802.11 wireless networks.
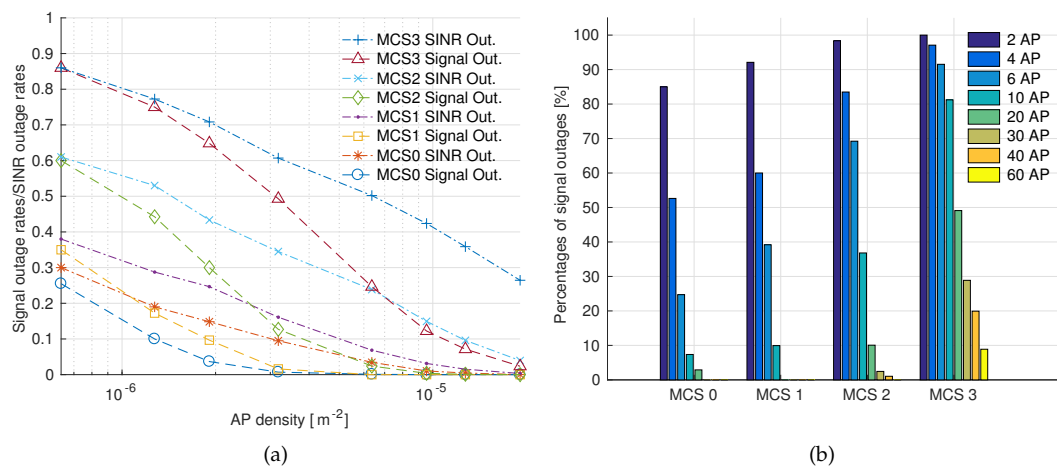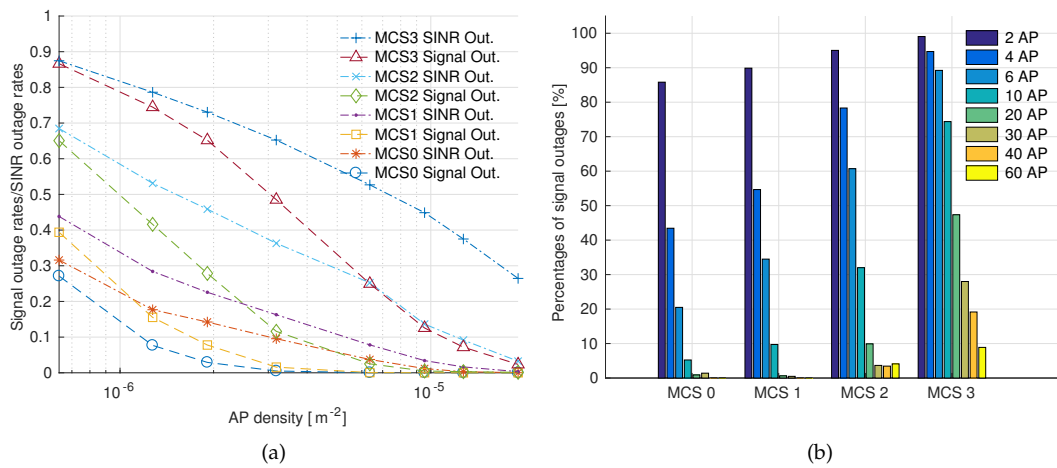

Figure 4. (**a**) Comparison of signal outage rates and SINR outage rates of users with different MCS levels and different numbers of APs. (**b**) Percentages of signal outage rates from SINR outage rates.

To better visualize the simulation results, in Figure 4b, we present bar graphs that show the percentages of the signal outage rates from the SINR outage rates when different MCS levels are used, and when varying numbers of APs are deployed. The bar graphs in Figure 4b, clearly show that the signal outages contribute most of the SINR outages, particularly with low AP numbers. The figure

also shows a pattern of higher signal outage percentages with higher MCS levels when the number of APs (referred to as AP in the figure) is fixed.

In Figure 5a, we show the simulation results of the signal outage rates and the SINR outage rates when the number of users is fixed at 60, while the number of APs increases from two to 60. Figure 5b shows the bar graphs of the data shown in Figure 5a. By comparing Figures 5a with 4a, and Figures 5b with 4b, we can see similar patterns between them, although the densities of users are quite different in the two cases.

(a)   (b)

Figure 5. (**a**) Comparison of signal outage rates and SINR outage rates of users when the number of users is fixed at 60. (**b**) Percentages of signal outage rates from SINR outage rates.

4. Heterogeneous Networks

For heterogeneous IEEE 802.11 wireless networks (i.e., IEEE 802.11 wireless networks composed of APs having different transmit powers), we consider only a two-tier case for simplicity. We call the tier-1 network a normal-cell, and the tier-2 network a small-cell because we assume that the APs of tier-1 networks use the transmit power P_{t1} of usual IEEE 802.11 APs (e.g., 100 mW), and that APs of tier-2 networks use smaller transmit powers P_{t2} than P_{t1}. We refer to users who are associated with the normal-cell APs as normal-cell users, and users who are associated with the small-cell APs as small-cell users.

The spatial distribution of the normal-cell APs is modeled using a homogeneous PPP of density λ_1, and the spatial distribution of the small-cell APs is modeled using another independent homogeneous PPP of density λ_2. The locations of the users are also distributed with another independent homogeneous PPP of density λ_u. We assume 100 mW as the transmit power of the normal-cell APs, P_{t1}, and 10 mW as the transmit power of the small-cell APs, P_{t2}. The transmit power of the users remains at 100 mW. Users are assumed to be connected to an AP having the strongest received signal strength before starting communication (i.e., unbiased, open access).

4.1. User Distances and Maximum Allowed Distances

The association probability of users with tier-n APs p_n within n-tier heterogeneous wireless networks is reported in [17]. Applying the results to our 2-tier heterogeneous wireless networks with

the fixed path-loss exponent $\alpha = 4$, the user association probabilities to normal-cells p_1 and small-cells p_2 can be respectively expressed as

$$p_1 = \left(1 + \frac{\lambda_2\sqrt{P_{t2}}}{\lambda_1\sqrt{P_{t1}}}\right)^{-1},$$

(11)

$$p_2 = \left(1 + \frac{\lambda_1\sqrt{P_{t1}}}{\lambda_2\sqrt{P_{t2}}}\right)^{-1}.$$

(12)

Using the normal-cell's user-association probability, we can find the CCDF and PDF of a random variable R_1 representing the distances of normal-cell users to their associated normal-cell APs by applying the results from [17], respectively, as given below:

$$
\begin{aligned}
P(R_1 > r) &= \frac{2\pi\lambda_1}{p_1} \int_r^\infty x e^{-\pi x^2 \left(\lambda_1 + \lambda_2\sqrt{P_{t2}/P_{t1}}\right)} dx \\
&= \frac{2\pi\lambda_1}{p_1} \frac{e^{-\lambda_1 \pi r^2 \left(1 + \frac{\lambda_2}{\lambda_1}\sqrt{P_{t2}/P_{t1}}\right)}}{2\pi\lambda_1 \left(1 + \frac{\lambda_2}{\lambda_1}\sqrt{P_{t2}/P_{t1}}\right)} \\
&= \frac{e^{-\lambda_1 \pi r^2 \left(1 + \frac{\lambda_2}{\lambda_1}\sqrt{P_{t2}/P_{t1}}\right)}}{p_1 \left(1 + \frac{\lambda_2}{\lambda_1}\sqrt{P_{t2}/P_{t1}}\right)} \\
&= e^{-\lambda_1 \pi r^2 / p_1},
\end{aligned}
$$

(13)

$$f_{R_1}(r) = \frac{2\pi\lambda_1}{p_1} r e^{-\lambda_1 \pi r^2 / p_1}.$$

(14)

Similarly, the CCDF and PDF of a random variable R_2 representing the distances between small-cell users and their associated small-cell APs can be expressed using the small-cell's user-association probability, respectively, as below:

$$
\begin{aligned}
P(R_2 > r) &= \frac{2\pi\lambda_2}{p_2} \int_r^\infty x e^{-\pi x^2 \left(\lambda_1 + \lambda_2\sqrt{P_{t1}/P_{t2}}\right)} dx \\
&= e^{-\lambda_2 \pi r^2 / p_2},
\end{aligned}
$$

(15)

$$f_{R_2}(r) = \frac{2\pi\lambda_2}{p_2} r e^{-\lambda_2 \pi r^2 / p_2}.$$

(16)

In addition, using the probability density function of a normal-cell user's distance from its associate normal-cell AP, we can find the expected distance of a normal-cell user to its associated AP, $E[R_1]$, as follows:

$$
\begin{aligned}
E[R_1] &= \frac{2\pi\lambda_1}{p_1} \int_0^\infty r^2 e^{-\lambda_1 \pi r^2 / p_1} dr \\
&= \frac{\pi\lambda_1}{p_1} p_1^{3/2} \frac{1}{2\pi\lambda_1^{\frac{3}{2}}} \\
&= \frac{\sqrt{p_1}}{2\sqrt{\lambda_1}}.
\end{aligned}
$$

(17)

Similarly, using the probability density function of a small-cell user's distance from its associated small-cell AP, we can express the expected distance of a small-cell user to its associated AP, $E[R_2]$, as follows:

$$E[R_2] = \frac{2\pi\lambda_1}{p_2} \int_0^\infty r^2 e^{-\lambda_2 \pi r^2 / p_2} dr$$
$$= \frac{\sqrt{p_2}}{2\sqrt{\lambda_2}}. \tag{18}$$

As an example, if we assume that $\lambda_1 = \lambda_2 = \lambda$, and apply the assumed transmit powers of APs for normal-cells and small-cells, the expected distances of normal-cell users and small-cell users from their associated APs can be respectively expressed as follows:

$$E[R_1] = \frac{(1 + \sqrt{1/10})^{\frac{1}{2}}}{2\sqrt{\lambda}}, \tag{19}$$

$$E[R_2] = \frac{(1 + \sqrt{10})^{\frac{1}{2}}}{2\sqrt{\lambda}}. \tag{20}$$

From the minimum received signal strength requirement of each MCS level P_k and the transmit power of normal-cell APs P_{t1}, we define the maximum allowed distance D_{k1} between a normal-cell user and its serving normal-cell AP for MCS level k as

$$D_{k1} = \left(\frac{P_k}{A \cdot E[h] \cdot P_{t1}} \right)^{-1/\alpha}$$
$$= \left(\frac{A \cdot E[h] \cdot P_{t1}}{\tau_k \cdot W} \right)^{1/\alpha}$$
$$= \left(\frac{A \cdot P_{t1}}{\tau_k \cdot W} \right)^{1/\alpha}. \tag{21}$$

Similarly, the maximum allowed distance D_{k2} between a small-cell user and its serving small-cell AP for MCS level k can be expressed using the transmit power of small-cell APs P_{t2} as

$$D_{k2} = \left(\frac{P_k}{A \cdot E[h] \cdot P_{t2}} \right)^{-1/\alpha}$$
$$= \left(\frac{A \cdot P_{t2}}{\tau_k \cdot W} \right)^{1/\alpha}. \tag{22}$$

Hence, from Equation (21), the maximum allowed distances of normal-cell users from their serving normal-cell APs can be calculated: about 894 m, 753 m, 502 m, and 284 m for MCS 0, MCS 1, MCS 2, and MCS 3, respectively. In addition, from Equation (22), the calculated maximum allowed distances of small-cell users from their serving small-cell APs are about 502 m, 423 m, 283 m, and 159 m for MCS 0, MCS 1, MCS 2, and MCS 3, respectively. These results are summarized in Table 3.

Table 3. Maximum allowed distances of normal-cell (P_{t1} = 100 mW) and small-cell (P_{t2} = 10 mW).

MCS Level k	Normal-Cell D_{k1} (m)	Small-Cell D_{k2} (m)
0	893.5	502.4
1	751.8	422.8
2	502.4	282.5
3	283.5	158.9

Table 3 clearly shows that the maximum allowed distances for the small-cells are smaller than those for the normal-cells with the same MCS level. In addition, we can see that the maximum allowed distances of normal-cells are the same as the maximum allowed distances for the homogeneous networks shown in Table 2. This is because we assume the same transmit power for the normal-cell APs as the transmit power of the APs in the homogeneous networks.

As a demonstration, in Figure 6a, we show the simulation results of the distances of normal-cell users and small-cell users from their associated APs when different numbers of users and different numbers of heterogeneous APs are randomly distributed in a circular area with a radius of 1000 m. For the simulations, both the number of normal-cell APs and the number of small-cell APs are increased from one to 30 (i.e., 1, 2, 3, 5, 10, 15, 20, and 30) while the number of users is fixed at 60. The simulation results are averaged values from 100-time repetitions with different seed values for randomness.

In Figure 6b, we also show the Voronoi diagram from one realization of PPPs with 30 normal-cell APs, 30 small-cell APs, and 60 users. The red arrows in the figure show the connectivity and directions of flows between normal-cell users and their serving normal-cell APs, and the blue arrows in the figure show the connectivity and directions of flows between small-cell users and their serving small-cell APs. The diagram is obtained after we add 30 small-cell APs and 30 more users to the homogeneous case in Figure 2b. From the figure, we can see small cells created by the small-cell APs.
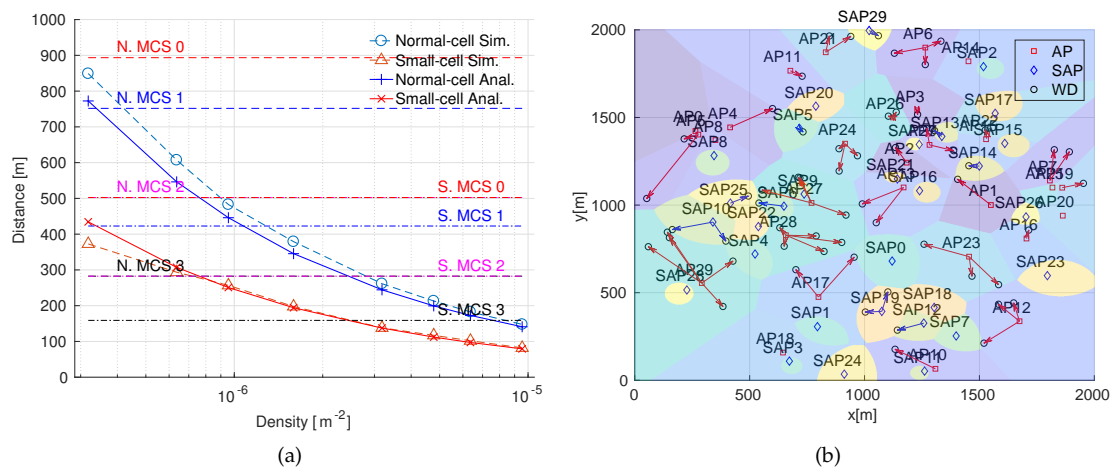
Figure 6. (**a**) Average distances between users and their serving APs in HetNets. (**b**) Voronoi diagram with 30 normal-cell APs, 30 small-cell APs (SAPs), and 60 wireless user devices (WDs).

As can be seen from Figure 6a, the simulation results follow the analyses for normal-cell users and small-cell users in Equations (19) and (20), respectively. In the figure, we also show the maximum allowed distances of the four MCS levels for normal-cells and small-cells with dashed and dash-dotted lines, respectively. From the figure, we can see that the maximum allowed distances for high MCS levels, such as MCS 2 and MCS 3, are not satisfied (on average) when AP densities are low in both normal-cells and small-cells. The simulations results and analytic data shown in Figure 6a indicate that when high MCS levels such as MCS 2 and MCS 3 are used, and when APs are sparsely distributed, signal outages can occur owing to the low received signal strengths in heterogeneous wireless networks regardless of whether users are connected to normal-cell APs or small-cell APs.

In addition, from the simulation results in Figure 6a, we can see that the average distances between the small-cell users and their serving small-cell APs follow the analysis more accurately than the normal-cell cases. The results indicate that the small-cell users experience less of the edge effect than the normal-cell users in the heterogeneous networks when independent PPPs are used for their locations in the bounded area. The results are also reflected in that the signal outages of the small-cell users follow the analysis for the heterogeneous networks more accurately as shown in

Section 4.2. We believe that this is caused by the finer granularity of the small-cells compared to the coarse granularity of the normal-cells.

4.2. Signal Outages

For a given density of normal-cell APs λ_1 and the minimum SINR requirement τ_k of MCS level k, we derive the probability of a signal outage for each MCS level k, PO_{k1}, of normal-cell users by combining Equations (21) and (13) as follows:

$$
\begin{aligned}
PO_{k1} &= P(R_1 > D_{k1}) \\
&= e^{-\lambda_1 \pi D_{k1}^2 / p_1} \\
&= e^{-\lambda_1 \pi \left(\frac{AP_{t1}}{\tau_k \cdot W} \right)^{\frac{2}{\alpha}} / p_1}.
\end{aligned}
\tag{23}
$$

Similarly, for small-cell users, the probability of a signal outage for each MCS level k, PO_{k2}, of small-cell users can be found by combining Equations (22) and (15) as follows:

$$
\begin{aligned}
PO_{k2} &= P(R_2 > D_{k2}) \\
&= e^{-\lambda_2 \pi \left(\frac{AP_{t2}}{\tau_k \cdot W} \right)^{\frac{2}{\alpha}} / p_2}.
\end{aligned}
\tag{24}
$$

Because we only consider the fixed path-loss exponent $\alpha = 4$, if we assume $\lambda_1 = \lambda_2 = \lambda$ and apply the assumed transmit powers of normal-cells and small-cells, Equations (23) and (24) respectively become

$$
PO_{k1} = e^{-\lambda \pi \left(1 + \sqrt{1/10}\right) \left(\frac{AP_{t1}}{\tau_k \cdot W} \right)^{\frac{1}{2}}},
\tag{25}
$$

$$
PO_{k2} = e^{-\lambda \pi \left(1 + \sqrt{10}\right) \left(\frac{AP_{t2}}{\tau_k \cdot W} \right)^{\frac{1}{2}}}.
\tag{26}
$$

Furthermore, from the relationship between Equations (11) and (12) as

$$
\begin{aligned}
\frac{p_2}{p_1} &= \frac{1 + \frac{\lambda_2}{\lambda_1} \frac{\sqrt{P_{t2}}}{\sqrt{P_{t1}}}}{1 + \frac{\lambda_1}{\lambda_2} \frac{\sqrt{P_{t1}}}{\sqrt{P_{t2}}}} \\
&= \frac{\frac{\lambda_2}{\lambda_1} \frac{\sqrt{P_{t2}}}{\sqrt{P_{t1}}} \left(1 + \frac{\lambda_2}{\lambda_1} \frac{\sqrt{P_{t2}}}{\sqrt{P_{t1}}} \right)}{\frac{\lambda_2}{\lambda_1} \frac{\sqrt{P_{t2}}}{\sqrt{P_{t1}}} + 1} \\
&= \frac{\lambda_2}{\lambda_1} \frac{\sqrt{P_{t2}}}{\sqrt{P_{t1}}},
\end{aligned}
\tag{27}
$$

we can conclude that PO_{k1} and PO_{k2} are equal when $\alpha = 4$, as follows:

$$
\begin{aligned}
&\frac{p_2}{p_1} = \frac{\lambda_2}{\lambda_1} \frac{\sqrt{P_{t2}}}{\sqrt{P_{t1}}} \\
\Rightarrow\ & \lambda_1 \sqrt{P_{t1}} / p_1 = \lambda_2 \sqrt{P_{t2}} / p_2 \\
\Rightarrow\ & -\lambda_1 \pi \left(\frac{AP_{t1}}{\tau_k \cdot W} \right)^{\frac{1}{2}} / p_1 = -\lambda_2 \pi \left(\frac{AP_{t2}}{\tau_k \cdot W} \right)^{\frac{1}{2}} / p_2 \\
\Rightarrow\ & e^{-\lambda_1 \pi \left(\frac{AP_{t1}}{\tau_k \cdot W} \right)^{\frac{1}{2}} / p_1} = e^{-\lambda_2 \pi \left(\frac{AP_{t2}}{\tau_k \cdot W} \right)^{\frac{1}{2}} / p_2} \\
\Rightarrow\ & PO_{k1} = PO_{k2}.
\end{aligned}
\tag{28}
$$

Equation (28) indicates that the signal outage probabilities of normal-cell users and small-cell users are not dependent on the PPP densities or the transmit powers of normal-cell APs and small-cell APs if the assumptions that we use in this paper are satisfied. Note that this result is also applicable to heterogeneous cellular networks because the signal outage probabilities are not related to specific medium access technologies. The result can be considered as a special case of the SINR outage probabilities for heterogeneous cellular networks analyzed in [17] by assuming no interference.

To evaluate the signal outage probabilities in heterogeneous wireless networks, in Figure 7a,b, we show the simulation results of the signal outage rates of the normal-cell users and the small-cell users, respectively, with different MCS levels and different λ values when $\lambda_1 = \lambda_2 = \lambda$. The numbers of both the normal-cell APs and the small-cell APs are increased from one to 30 (i.e., 1, 2, 3, 5, 10, 15, 20, and 30) in a circular area having a radius of 1000 m. The number of users is fixed at 60. The signal outage rates are averaged values of the percentage of the signal-outage users obtained from among all the users of the same tier from 100-time repetitions.
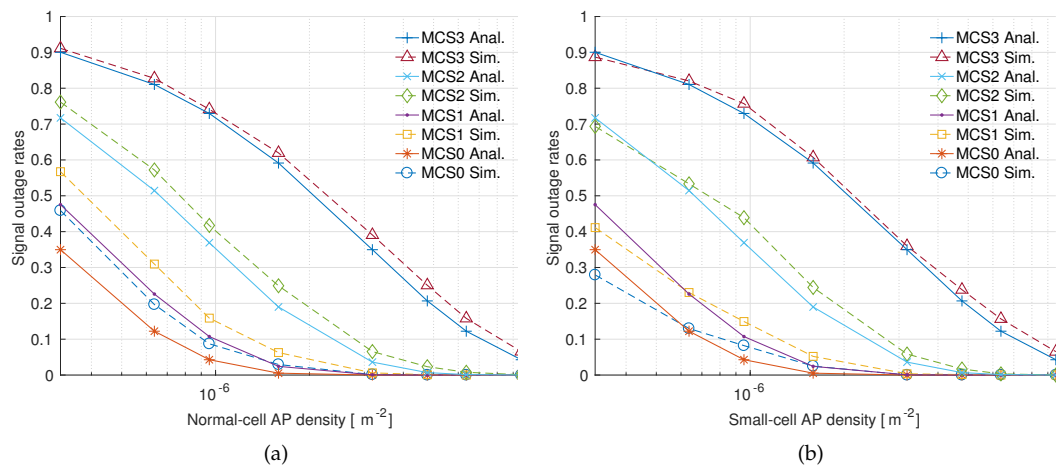
Figure 7. Signal outage rates of normal-cell users (**a**) and small-cell users (**b**) when $\lambda_1 = \lambda_2$.

From Figure 7a, we can see that the simulation results of the signal outage rates of the normal-cell users follow the analytic data from Equation (25). The simulation results of the signal outage rates of the small-cell users and the analytic data from Equation (26) in Figure 7b also show matches. In addition, by comparing the simulation results in Figure 7a,b, we can see that the signal outages of the small-cell users follow the analysis more accurately than those of the normal-cell users as expected by the better accuracy in the estimated distances between the small-cell users and their serving APs as shown in Figure 6a.

To verify the independence of the signal outages from the densities of heterogeneous APs, in Figure 8a,b, we show the simulation results of heterogeneous wireless networks after changing the densities of APs for small-cells to twice those of normal-cells (i.e., $\lambda_2 = 2\lambda_1$): We increased the number of normal-cell APs from one to 30 (i.e., 1, 2, 3, 5, 10, 15, 20, and 30) as before, but the number of small-cell APs was increased from two to 60 (i.e., 2, 4, 6, 10, 20, 40, and 60) in the same topology (a circular area with a radius of 1000 m). The number of users was again fixed at 60.

Figure 8a shows the simulation results of the signal outages of the normal-cell users along with the analytic data from Equation (23). Figure 8b shows the simulations results of the signal outage rates of the small-cell users along with the analytic data from Equation (24). From the figures, we can see that the simulation results match the estimated signal outage probabilities for the heterogeneous networks, which are similar to the results in Figure 7a,b. The figures also show that signal outage probabilities are not dependent on the densities of APs of normal-cells and small-cells, as indicated by Equation (28).
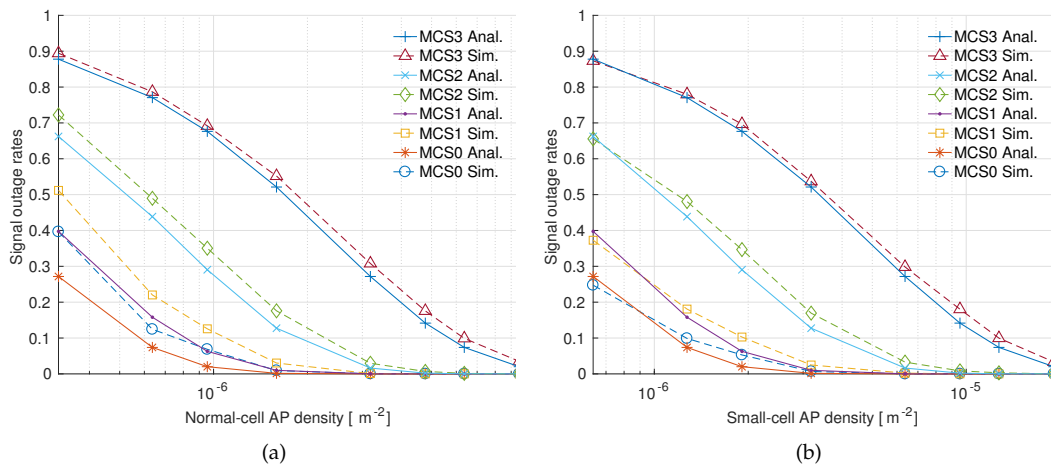
Figure 8. Signal outage rates of normal-cell users (**a**) and small-cell users (**b**) when $\lambda_2 = 2\lambda_1$.

4.3. Comparison with SINR Outages

To investigate the impact of signal outages on SINR outages in heterogeneous networks, we use the same approach used for homogeneous networks with ns-2 simulations as in Section 3.3. We increase the number of both the normal-cell APs and the small-cell APs from one to 30 (i.e., 1, 2, 3, 5, 10, 15, 20, and 30) in a circular area with a radius of 1000 m. The number of users is fixed at 60. For each scenario, we calculated the average values of the signal outage rates and the SINR outage rates of normal-cell users and small-cell users separately from 100-time repetitions.

In Figures 9a and 10a, we show the simulation results of the signal outage rates and the SINR outage rates of normal-cell users and the small-cell users, respectively, with different MCS levels and different AP densities in heterogeneous IEEE 802.11a wireless networks. For better visualization, in Figures 9b and 10b, we also show the bar graphs of the percentages of the signal outage rates obtained from the SINR outage rates using the data shown in Figures 9a and 10a, respectively. From the simulation results in the figures, we can see that a large percentage of the SINR outages are caused by the signal outages, regardless of whether the tiers of the cells that users are connected to have high MCS levels being used with low AP densities, which is similar to the results obtained for homogeneous networks.
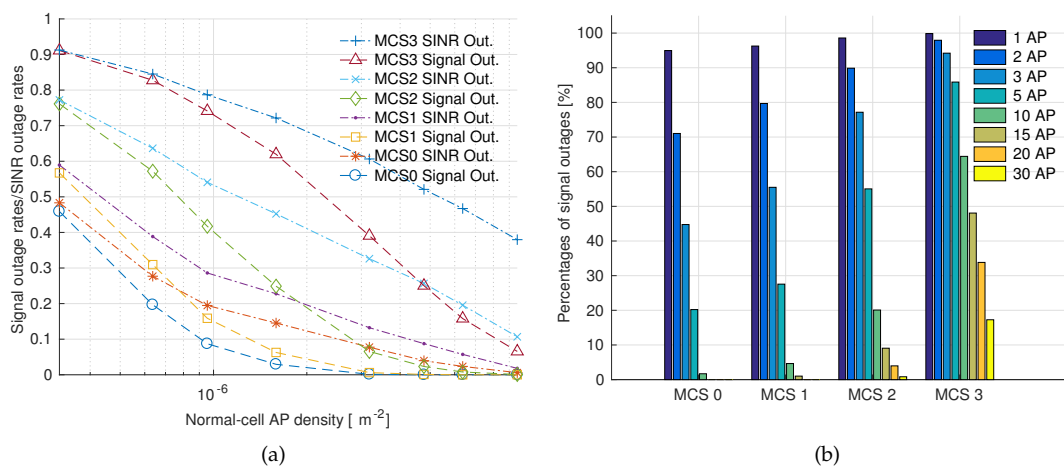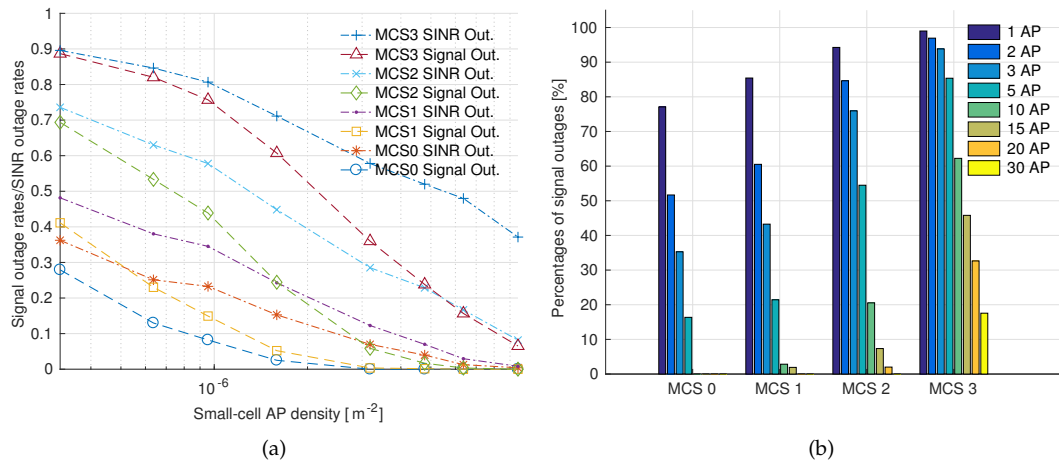

Figure 9. (**a**) Comparison of signal outage rates and SINR outage rates of normal-cell users. (**b**) Percentages of signal outage rates from SINR outage rates of normal-cell users.
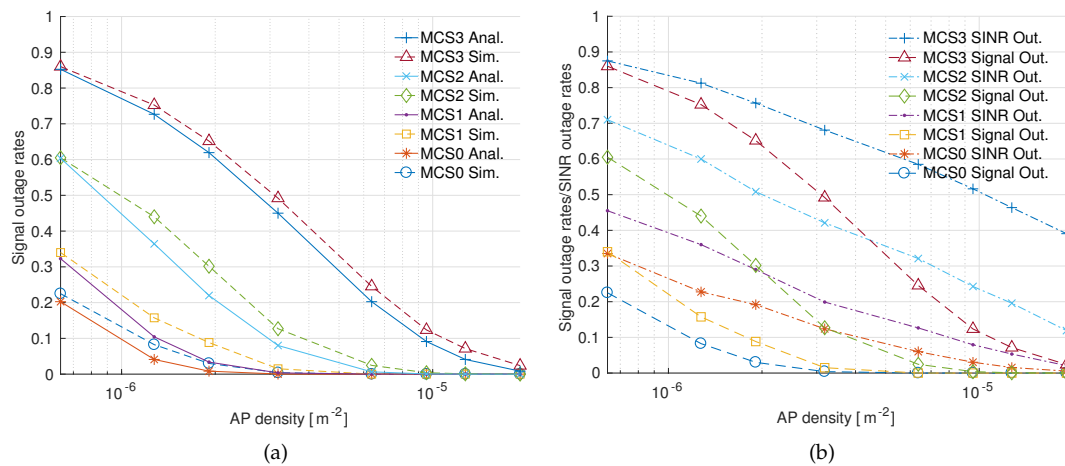
Figure 10. (**a**) Comparison of signal outage rates and SINR outage rates of small-cell users. (**b**) Percentages of signal outage rates from SINR outage rates of small-cell users.

However, by comparing the signal outage percentages of small-cell users in Figure 10b with those of normal-cell users in Figure 9b, we can see that small-cells show less signal outage percentages than those of the normal-cells, especially when the numbers of APs and the MCS levels are low. This result can also be attributed to the fact that small-cells experience less of the edge effect compared to normal-cells as shown in Figure 6a.

5. The Effects of Rayleigh Fading and RTS/CTS

In this section, we show simulation results when Rayleigh fading is applied to the transmitted signal strengths, as well as the simulation results when the RTS/CTS scheme is enabled by all participating nodes in simulations.

In Figure 11, we show the simulation results with the Rayleigh fading. For the simulations, we increased both the number of APs and the number of users from two to 60 (i.e., 2, 4, 6, 10, 20, 30, 40, and 60) in a circular area with a radius of 1000 m. The simulation results are averaged values from 100-time repetitions. Figure 11a shows the simulation results of the signal outage rates along with the analysis results of the signal outages. Figure 11b shows the signal outage rates of users and the SINR outage rates of users together.

Figure 11. (**a**) Signal outage rates with Rayleigh fading. (**b**) Comparison of signal outage rates and SINR outage rates with Rayleigh fading.

By comparing the simulation results in Figures 11a with 3a in Section 3, we can see that they are not much different from each other. This result could be expected because the signal outage rates of users we measure from the simulations are based on the averaged values of the signal strengths when packets arrive at their target nodes during the simulation time, and we assume unit mean for the Rayleigh fading (i.e., $h \sim exp(1)$) in the radio transmission model of Equation (1). However, by comparing Figures 11b with 4a, we can see increases in the SINR outage rates when the Rayleigh fading is applied. This can be attributed to the randomness in the received signal strengths by the Rayleigh fading.

In Figure 12, we show the simulation results when the RTS/CTS scheme is enabled. Both the number of APs and the number of users are increased from two to 60 (i.e., 2, 4, 6, 10, 20, 30, 40, and 60) in a circular area with a radius of 1000 m. Figure 12a shows the simulation results of the signal outage rates of users with different AP densities and different MCS levels. Figure 12b shows both the signal outage rates of users and the SINR outage rates of users. From the simulation results in Figure 12a,b, we can see that they are not much different from the simulation results without RTS/CTS shown in Figures 3a and 4a, respectively. This result indicates that most interference in the simulated scenarios comes from the nodes outside the carrier sensing range of CSMA/CA. (In our simulations, the carrier sensing range is about 532 m because `CSThresh_` parameter was set to −112 dBW.)
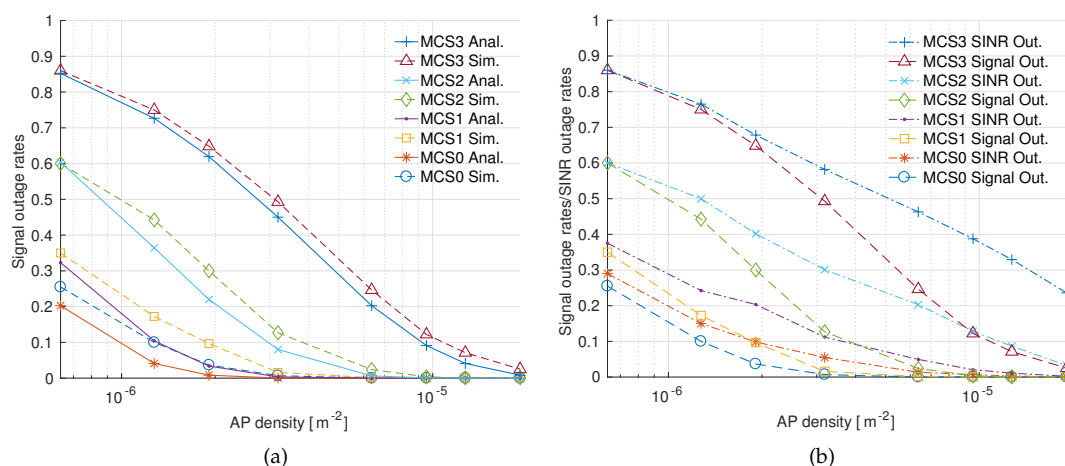
Figure 12. (**a**) Signal outage rates when RTS/CTS is enabled. (**b**) Comparison of signal outage rates and SINR outage rates when RTS/CTS is enabled.

6. Conclusions

This paper investigates the signal outages that users may experience in CSMA/CA-based wireless networks. Using homogeneous Poisson point processes, we analyzed the signal outage probabilities of randomly distributed users when different numbers of access points are randomly distributed in a given area, and different MCS levels are used for communication between them. We validated the analysis by showing the rates of the signal-outage users among the total number of users through extensive simulations. We also analyzed the signal outage probabilities of users in heterogeneous wireless networks where APs with two different transmit powers are mixed in a given area. From the simulation results of the heterogeneous networks, we found that the distances between small-cell users and their serving APs follow the analysis more accurately than the normal-cell cases.

Using extensive event-driven simulations, we showed that a significant percentage of the SINR outages is caused by the signal outages when the densities of APs are low or when high MCS levels are used for communication between APs and users in both homogeneous and heterogeneous wireless networks. Furthermore, using simulations and analysis, we showed the equality in the signal outage

probabilities of normal-cell users and small-cell users in heterogeneous wireless networks if the assumptions we use in this paper are satisfied.

We expect that the signal outage probabilities investigated in this paper can be used for future studies in CSMA/CA-based wireless networks, and in the development of relatively large-scale IEEE 802.11 wireless networks. As a future work, we consider incorporating other IEEE standards such as IEEE 802.11g and IEEE 802.11n, as well as reflecting the carrier frequencies of IEEE 802.11 standards for the radio transmission modeling and simulations.

Conflicts of Interest: The authors declare no conflict of interest.

References

1. Atzori, L.; Iera, A.; Morabito, G. The Internet of Things: A survey. *Comput. Netw.* **2010**, *54*, 2787–2805.
2. Kang, W.M.; Moon, S.Y.; Park, J.H. An enhanced security framework for home appliances in smart home. *Hum.-Centric Comput. Inf. Sci.* **2017**, *7*, doi:10.1186/s13673-017-0087-4.
3. Sharma, P.; Moon, S.Y.; Park, J.H. Block-VN: A distributed blockchain based vehicular network architecture in smart City. *J. Inf. Proc. Syst.* **2017**, *13*, 184–195.
4. Maity, S.; Park, J.H. Powering IoT devices: A novel design and analysis technique. *J. Converg.* **2016**, *7*, 16071001.
5. Stankovic, J.G. Research directions for Internet of Things. *IEEE Internet Things J.* **2014**, *1*, 3–9.
6. IEEE Computer Society. *IEEE Std 802.11-2016 Part 11: Wireless LAN Medium Access Control (MAC) and Physical Layer (PHY) Specifications*; IEEE Comput. Soc.: Washington, DC, USA, 2016.
7. IEEE Computer Society. *IEEE Std 802.15.4-2015: IEEE Standard for Low-Rate Wireless Networks*; IEEE Computer Society: Washington, DC, USA, 2015.
8. Yonhap NEWS Agency. Seoul to Provide Free Wi-Fi at All Public Places by 2017, 2016. Available online: http://english.yonhapnews.co.kr/news/2016/02/23/0200000000AEN20160223009200315.html (accessed on 23 March 2018).
9. Shen, J.; Cao, J.; Liu, X.; Zhang, C. DMAD: Data-driven measuring of Wi-Fi access point deployment in urban space. *ACM Trans. Intell. Syst. Technol.* **2017**, *9*, 1–29.
10. NGMN (Next Generation Mobile Networks) Alliance, NGMN 5G White Paper, 2015. Available online: https://www.ngmn.org/fileadmin/ngmn/content/downloads/Technical/2015/NGMN_5G_White_Paper_V1_0.pdf (accessed on 8 May 2018).
11. Andrews, J.G. Seven ways that HetNets are a cellular paradigm shift. *IEEE Commun. Mag.* **2013**, *51*, 136–142.
12. Chiu, S.; Stoyan, D.; Kendall, W.S.; Mecke, J. *Stochastic Geometry and Its Applications*, 3rd ed.; Wiley: New York, NY, USA, 2013.
13. Haenggi, M. *Stochastic Geometry for Wireless Networks*; Cambridge University Press: Cambridge, UK, 2012.
14. Andrews, J.G.; Baccelli, F.; Ganti, R.K. A tractable approach to coverage and rate in cellular networks. *IEEE Trans. Commun.* **2011**, *59*, 3122–3134.
15. Weber, S.; Andrews, J.G.; Jindal, N. An overview of the transmission capacity of wireless networks. *IEEE Trans. Commun.* **2010**, *58*, 3593–3604.
16. Yu, S.M.; Kim, S.-L. Downlink Capacity and Base Station Density in Cellular Networks, International Symposium on Modeling & Optimization in Mobile. In Proceedings of the 2013 11th International Symposium on Modeling & Optimization in Mobile, Ad Hoc & Wireless Networks (WiOpt), Tsukuba Science City, Japan, 13–17 May 2013.
17. Jo, H.-S.; Sang, Y.J.; Xia, P.; Andrews, J.G. Heterogeneous cellular networks with flexible cell association: A comprehensive downlink SINR analysis. *IEEE Trans. Wirel. Commun.* **2012**, *11*, 3484–3495.
18. Singh, S.; Dhillon, H.S.; Andrew, J.G. Offloading in heterogeneous networks: Modeling, analysis, and design insights. *IEEE Trans. Wirel. Commun.* **2013**, *12*, 2484–2497.
19. Sang, Y.J.; Kim, K.S. Load distribution in heterogeneous cellular networks. *IEEE Commun. Lett.* **2014**, *18*, 237–240.

20. Jo, H.-S.; Xia, P.; Andrews, J.G. Open, closed, and shared access femtocells in the downlink. *EURASIP J. Wirel. Commun. Netw.* **2012**, *2012*, 363.

21. Naghshin, V.; Rabiei, A.M.; Beaulieu, N.C.; Maham, B. Accurate Statistical Analysis of a Single Interference in Random Networks with Uniformly Distributed Nodes. *IEEE Commun. Lett.* **2014**, *18*, 197–200.

22. Babich, F.; Comisso, M. Including the angular domain in the analysis of finite multi-packet peer-to-peer networks with uniformly distributed sources. *IEEE Trans. Commun.* **2016**, *64*, 2494–2510.

23. Babich, F.; Comisso, M.; Crismani, A.; Dorni, A. On the design of MAC protocols for multi-packet communication in IEEE 802.11 heterogeneous networks using adaptive antenna arrays. *IEEE Trans. Mobile Comput.* **2015**, *14*, 2332–2348.

24. Mordachev, V.; Loyka, S. On node density—Outage probability tradeoff in wireless networks. *IEEE J. Sel. Areas Commun.* **2009**, *27*, doi:10.1109/JSAC.2009.090909.

25. Bettstetter, C.; Resta, G.; Santi, P. The node distribution of the random waypoint mobility model for wireless ad hoc networks. *IEEE Trans. Mobile Comput.* **2003**, *2*, 257–269.

26. Gong, Z.; Haenggi, M. Interference and outage in mobile random networks: Expectation, distribution, and correlation. *IEEE Trans. Mobile Comput.* **2014**, *13*, 337–349.

27. Nguyen, H.Q.; Baccelli, F.; Kofman, D. A Stochastic Geometry Analysis of Dense IEEE 802.11 Networks. In Proceedings of the IEEE INFOCOM 2007 26th IEEE International Conference on Computer Communications, Barcelona, Spain, 6–12 May 2007.

28. Haenggi, M. Mean Interference in Hard-core Wireless Networks. *IEEE Commun. Lett.* **2011**, *15*, 792–794.

29. Alfano, G.; Garetto, M.; Leonardi, E. New directions into the stochastic geometry analysis of dense CSMA network. *IEEE Trans. Mobile Comput.* **2014**, *13*, 324–336.

30. ElSawy, H.; Hossain, E. A modified hard core point process for analysis of random CSMA wireless networks in general fading environments. *IEEE Trans. Commun.* **2013**, *61*, 1520–1534.

31. Zhou, Z.; Li, L.; Xu, Y. Energy Efficient Cloud Computing Environment via Autonomic Meta-director Framework. In Proceedings of the WiCom 2009 5th International Conference on Wireless Communications, Networking and Mobile Computing, Beijing, China, 24–26 September 2009.

32. Aldawsari, B.; Baker, T.; England, D. Trusted Energy-Efficient Cloud-Based Services Brokerage Platform. *Int. J. Intell. Comput. Res.* **2015**, *6*, 630–639.

33. Baker, T.; Ngoko, Y.; Tolosana-Calasanz, R. An Efficient Energy Routing Algorithm Based on Dynamic Programming in Wireless Sensor Networks. In Proceedings of the International Conference on Developments of E-Systems Engineering, Abu Dhabi, UAE, 16–18 December 2013.

34. Baker, T.; Al-Dawsari, B.; Tawfik, H.; Reid, D.; Ngoko, Y. GreeDi: An energy efficient routing algorithm for big data on cloud. *Ad Hoc Netw.* **2015** *35*, 83–96.

35. The Network Simulator—ns-2. Available online: http://www.isi.edu/nsnam/ns (accessed on 26 March 2018).

36. Chen, Q.; Schmidt-Eisenlohr, F.; Jiang, D. Overhaul of IEEE 802.11 Modeling and Simulation in NS-2. In Proceedings of the 10th ACM Symposium on Modeling, Analysis, and Simulation of Wireless and Mobile Systems, Chania, Crete Island, Greece, 22–26 October 2007; pp. 159–168.

37. IEEE Computer Society. *IEEE Std 802.11a-1999 Part 11: Wireless LAN Medium Access Control (MAC) and Physical Layer (PHY): High-Speed Physical Layer in the 5 GHZ Band*; IEEE Computer Society: Washington, DC, USA, 1999.

38. Schmidt-Eisenlohr, F. *Interference in Vehicle-to-Vehicle Communication Networks—Analysis, Modeling, Simulation and Assessment*; KIT Scientific Publishing: Karlsruhe, Germany, 2010.

39. Chen, Q.; Schmidt-Eisenlohr, F.; Jiang, D.; Torrent-Moreno, M.; Delgrossi, L.; Hartenstein, H. Overhaul of IEEE 802.11 Modeling and Simulation in NS-2 (802.11Ext). Available online: https://dsn.tm.kit.edu/medien/downloads_old/Documentation-NS-2-80211Ext-2008-02-22.pdf (accessed on 26 March 2018).

40. ElSawy, H.; Hossain, E.; Haenggi, M. Stochastic geometry for modeling, analysis, and design of multi-tier and cognitive cellular wireless networks: A Survey. *IEEE Commun. Surv. Tutor.* **2013**, *15*, 996–1019.

41. Two-Ray Ground Reflection Model in NS Version 2 Manual. Available online: http://www.isi.edu/nsnam/ns/doc/node218.html (accessed on 26 March 2018).

42. Okabe, A.; Boots, B.; Sugihara K.; Chiu, S.N. *Spatial Tessellations: Concepts and Applications of Voronoi Diagrams*; Wiley: New York, NY, USA, 2000.
43. NO Ad-hoc Routing Agent. Available online: http://icapeople.epfl.ch/widmer/uwb/ns-2/noah (accessed on 26 March 2018).